# COMPUTATIONAL GEOMETRY PROVIDES INDIRECT EVIDENCE OF DARK MATTER LOCATION IN COSMIC STRUCTURES

**Arturo Tozzi** (Corresponding Author)
Center for Nonlinear Science, University of North Texas
1155 Union Circle, #311427
Denton, TX 76203-5017, USA
tozziarturo@libero.it

**James F. Peters**
Department of Electrical and Computer Engineering, University of Manitoba
75A Chancellor's Circle
Winnipeg, MB R3T 5V6, Canada
james.peters3@umanitoba.ca

**Sheela Ramanna**
Department of Applied Computer Science, University of Winnipeg
Winnipeg, Manitoba R3B 2E9, Canada
s.ramanna@uwinnipeg.ca

## ABSTRACT

The elusive dark matter is the best candidate in order to explain gravitational effects such as, for example, the motion of stars in galaxies. We introduce a novel method for the measurement of information in cosmic images called maximal nucleus clustering (MNC) *i.e.*, nucleus clustering's Rényi entropy derived from strong proximities in feature-based Voronoï tessellations. MNC is a novel, fast and inexpensive image-analysis technique, independent from other detectable signals. It permits the assessment of changes in gradient orientation into zones of two-dimensional cosmic images that generally are not taken into account by other techniques. In order to evaluate the potential applications of MNC, we looked for the presence of MNC's distinctive hallmarks in the plane surface of astronomic images. We found that Rényi entropy is higher in MNC areas of cosmic images than in the surrounding regions, and that these patterns are correlated with cosmic zones containing a lesser amount of dark energy. Therefore, computational geometry provides a bridge made of affine connexions and proximities between features of a two-dimensional pictures and physical features of the Universe.

**KEYWORDS:** topology; black holes; galaxy; Borsuk-Ulam theorem.

A diffuse presence of invisible dark matter in the Universe is required by current cosmological models, in order to explain features such as the experimentally detected movement of stars in the peripheries of galaxies (Penrose, 2011; Aad et al., 2013; Khachatryan et al, 2015). Here we introduce a novel technique of cosmic image analysis in the plane surface of 2D images. The method, called computational proximity, takes into account maximal nucleus clustering in Voronoï tessellations (Peters, 2016, Peters and Inan, 2016). Cosmic images are subdivided in contiguous polygons, termed "Voronoï polygons" (without interstices or overlap). They yield a density map, called "tessellation", that makes it possible to make an objective measurement of the spatial distribution of polygon areas and helps to define "random", "regular" and "clustered" distributions (Franck and Hart, 2010; Edelsbrunner, 2014; Peters and Guadagni, 2015; Peters et al., 2016). Voronoï tessellations have been already used in cosmology, *i.e.*, in order to to investigate spatial cosmic matter distribution on scales of a few up to more than a hundred Megaparsec (van de Weygaert, 2007). In a Voronoï tessellation of a cosmic image, of particular interest is the presence of maximal nucleus clusters (MNC), *i.e.*, cosmic zones with the highest number of adjacent polygons (Peters and Inan, 2016). The MNC clustering approach includes a main feature of level set methods, namely, a nucleus boundary that is embedded in a family of nearby level sets (Saye and Sethian, 2011). MNC reveals regions of the Universe, independent from other techniques, characterized by different gradient orientation and gradient magnitude (edge strength) of region pixels. Here we evaluate the power and potentialities of this novel, easy and inexpensive approach. We also establish a link between MNCs and the presence of the otherwise undetectable dark matter in cosmic images.

**MATERIALS AND METHODS**

**Cosmic images**. We used public domain astronomic pictures from the NASA website (http://apod.nasa.gov/apod/archivepix.html). Here follows a list of the cosmic structures we evaluated using computational geometry techniques.

1) Starburst Galaxy Messier 94 (**Figure 1**). It lies 15 million light-years distant in the northern constellation of Canes Venatici. The galaxy's compact nucleus and prominent inner dust lanes are surrounded by a ring of young, massive stars, likely less than 10 million years old (Image Credit: ESA/Hubble and NASA).

2) The "classical" image depicting the cosmic microwave background (**Figure 2A**), which is the almost isotropic thermal radiation left over from an early stage in the development of the Universe, about 380,000 years after the Big Bang (Penzias and Wilson, 1965; Gawiser and Silk, 2000; Fixsen, 2009).

3) the SDSS 3-dimensional map of the distribution of galaxies (**Figure 2B**). Earth is at the center, and each point represents a galaxy, containing about 100 billion stars. The outer circle is at a distance of two billion light years. Both slices contain all galaxies within -1.25 and 1.25 degrees declination. (Image Credit: M. Blanton and the Sloan Digital Sky Survey, https://www.sdss3.org/science/gallery_sdss_pie2.php).

4) Cosmic structures from the in the long-necked, northern constellation of Camelopardalis. In particular, we evaluated the the spiral galaxy NGC 2403 (**Figure 3A**), which stands within the boundaries of the constellation (Image Credit & Copyright: Eric Coles and Mel Helm), and the Hidden Galaxy IC 342 (**Figure 3B**), similar in size to large spiral galaxies in our neighborhood. IC 342 may have undergone a recent burst of star formation activity and has gravitationally influenced the evolution of the Milky Way (Image Credit & Copyright: Fabiomassimo Castelluzzo).

5) IRG-NGC303, magnitude 14.3, lenticular Galaxy (**Figure 3C**).

6) the Red Square Nebula MWC9 22 (**Figure 4**). The featured image combines infrared exposures from the Hale Telescope on Mt. Palomar in California, and the Keck-2 Telescope on Mauna Kea in Hawaii. A hypothesis for the unusual square shape is that the central stars expelled cones of gas during their late developmental stage. These cones incorporated nearly right angles and were visible from the sides. Supporting evidence for the cone hypothesis includes radial spokes in the image that might run along the cone walls. (Image Credit & Copyright: Peter Tuthill & James Lloyd).

7) NGC 1068 (**Figure 5A**). This spiral galaxy, located in the Cetus constellation 47 million light-years away, contains a supermassive black hole (detected by NASA's Nuclear Spectroscopic Telescope Array, or NuSTAR, and the European Space Agency's XMM-Newton space observatory).

8) Markarian 231 (**Figure 5B**). This Hubble Space Telescope image reveals a bright glow in the center of the interacting galaxy Markarian 231, the nearest quasar to the Earth. Quasars are powered by a central black hole that heats gas around it to unleash tremendous amounts of energy. Hubble spectroscopic observations infer the presence of two supermassive black holes whirling around each other (Credit: NASA, ESA, the Hubble Heritage Team (StScI/AURA)-ESA/Hubble Collaboration, and A. Evans (University of Virginia, Charlottesville/NRAO/Stony Brook University).

9) SDSSJ1126-2944 (**Figure 5C**). This galaxy is the result of a merger between two smaller galaxies, which brought together a pair of supermassive black holes. One of the black holes is surrounded by a typical amount of stars, while the other is strangely "naked" and has a much lower number of associated stars than expected (Comerford 2015). (Image Credit & Copyright: Julie Comerford and NASA Chandra Xray Observatory).

**Nucleus clustering in Voronoï tessellations**. The plane surfaces of cosmic structures' pictures were subdivided into contiguous polygons, the so-called "Voronoï polygons" (**Figure 1A**). Geometrically, a Voronoï tessellation is a collection of non-overlapping convex polygons (Edelsbrunner, 2006). Each point $p$ in the tiling represents a generating point (called a site) with particular features, such as corners, centroids, gradient orientation and brightness (some of them are depicted with the letter $p$ in **Figure 1A**). A Voronoï region contains every point in the plane that is closer to the point $p$ than to any other site. In technical words, each polygon is a Voronoï region $V(s)$ of a generating point $s \in S$, which is a set of all points nearer $s$ than to any other point in $S$. We achieve a "tessellation", *i.e.*, a density map that allows an objective measurement of the polygon areas' spatial distribution. A central Voronoï region in called the cluster nucleus (some of of the cluster nuclei are depicted with the letter N in **Figure 1A**) and contains all the points on the plane surface that are nearer to the generating point $p$ than to any other generating point on the surface (**Figure 1B**). A *Voronoï nucleus cluster* is a collection of Voronoï polygons that are adjacent to their central cluster nucleus (Peters, 2016): that is, each polygon which is strongly near a cluster nucleus has an edge in common with its polygon (Edelsbrunner, 2014). In a Voronoï tessellation carried out in a so called "strong" proximity space (Peters 2016), of particular interest is the presence of maximal nuclei, *i.e.*, zones with the highest number of sides and of adjacent polygons (**Figure 1C,** letter M). The maximal nucleus plus its adjacent polygons is called maximal nucleus cluster (MNC): in sum, the latter is a Voronoï cluster in which the cluster nucleus is a polygon which displays the highest number of sides (in **Figure 1E,** a MNC is embedded in the white oval). In technical terms, this clustering approach includes a main feature of level set methods,

namely, a nucleus boundary that is embedded in a family of nearby level sets. Strongly near Voronoï polygons is an application of the notion of strong proximity between sets of points: for further details and the algorithms, see Peters (2016) and Peters and Inan (2016).

Summarizing, in a tessellated image, Voronoï tessellation serve as indicator of high object concentration and inhomogeneity distributions, while MNCs as indicators of gradient orientations.

**Steps to Construct Maximal Nucleus Clusters on a Tessellated Cosmic Image.** Here we give the steps to construct MNCs on a tessellated cosmic image (see **Figure 1.0**). The basic approach is to find those polygonal regions in a cosmic image that yield the most information and the reflect the fact that the site (generating point) each Voronoï region has a gradient orientation and gradient magnitude (edge strength) that is different from all of the other generating points. The nucleus of an MNC has a singular character, since the number of Voronoï regions along the borders of the nucleus is maximal. It is this maximality that is a signature of cosmic regions that yield the greatest information levels.

---

**Algorithm 1: Construct Cosmic Maximal Nucleus Cluster**

> **Input** : Cosmic image $img$.
> **Output**: MNCs on cosmic image $img$.
> 1   $img \longmapsto TitledImg$/*(Voronoï tessellation)*/;
> 2   *Choose a Voronoï region in TitledImg:* *;
> 3   $ngon \longleftarrow TiledImg$;
> 4   $NoOfSides \longleftarrow ngon$;
> 5   /* Count no. of sides in $ngon$ & remove it from $TitledImg$. */;
> 6   $TiledImg := TiledImg \smallsetminus ngon$;
> 7   $ContinueSearch := True$;
> 8   **while** *(TiledImg $\neq \varnothing$ and ContinueSearch)* **do**
> 9      $ngonNew \longleftarrow TiledImg$;
> 10      $TiledImg := TiledImg \smallsetminus ngonNew$;
> 11      $NewNoOfSides \longleftarrow ngonNew$;
> 12      **if** $(NewNoOfSides > NoOfSides)$ **then**
> 13         $ngon := ngonNew$;
> 14      **else**
> 15         /* Otherwise ignore $ngonNew$: */
> 16      **if** $(TiledImg = \varnothing)$ **then**
> 17         $ContinueSearch := False$;
> 18         $maxN := ngon$;
> 19         /* Cosmic image MNC found; Discontinue search */;

---

**Figure 1.0.** The steps in the method used to construct the mesh MNCs on a cosmic image shown in **Figure 1D**.

**Rényi entropy assessed information content in cosmic Nucleus Clusters.** We showed in the previous paragraphs that the major new elements in the evaluation of cosmic images are nucleus clusters, maximal nucleus clusters, strongly near maximal nucleus clusters, *e.g.*, convexity structures that occur whenever max nucleus clusters intersect (Peters and Inan, 2016). In a Voronoï tessellation, of particular interest is the presence of ***maximal nucleus clusters*** (MNC), *i.e.*, clusters with the highest number of adjacent polygons. In this section, we introduce a measure of the information that MNCs in cosmic images yield. We demonstrate that MNC reveal regions of the Universe with higher levels of information, in comparison with non-MNC regions, that uniformly yield less information.

3

In a series of papers, Rényi (Rènyi, 1961; Rènyi, 1966), introduced a measure of information of a set random events. Let $X$ be a set random events such as the occurrence of polygonal areas in a Voronoï tessellation and let $\beta > 0, \beta \neq 1, p(x)$ the probability of the occurrence of $x$ in $X$. Then Rényi entropy $H_\beta(X)$ is defined by

$$X = \{x_1, \cdots, x_n\},$$

$$H_\beta(X) = \frac{1}{1-\beta} \log_2 \sum_{i=1}^{n} p^\beta(x_i).$$

Because of the relationship between Rényi entropy of a set of events and the information represented by events, Rényi entropy and information are interchangeable in practical applications (Rènyi, 1982; Bromiley et al., 2010). In fact, it has been shown that Rényi entropy $H_\beta(X)$ is a monotonic function of the information associated with $X$. This means that Rényi entropy can be used as a measure of information for any order $\beta > 0$.

Let $X_{MNC}, X_{nonMNC}$ be sets of MNC polygon areas and non-MNC polygon areas in a random distribution of tessellation polygon areas. Also, let $p(x) = \frac{1}{x}, p(y) = \frac{1}{y}$ be the probability of occurrence of $x \in X_{MNC}, y \in X_{nonMNC}$. Notice that the nuclei in MNCs have the highest concentration of adjacent polygons, compared with non-MNC polygons. Based on measurements of Rényi entropy for MNC vs. non-MNC observations, we have confirmed that Rényi entropy of nucleus polygon clusters is consistently higher than the set of non-MNC polygons (**Figures 3** and **4**). This finding indicates that MNCs yield higher information than any of the polygon areas outside the MNCs.
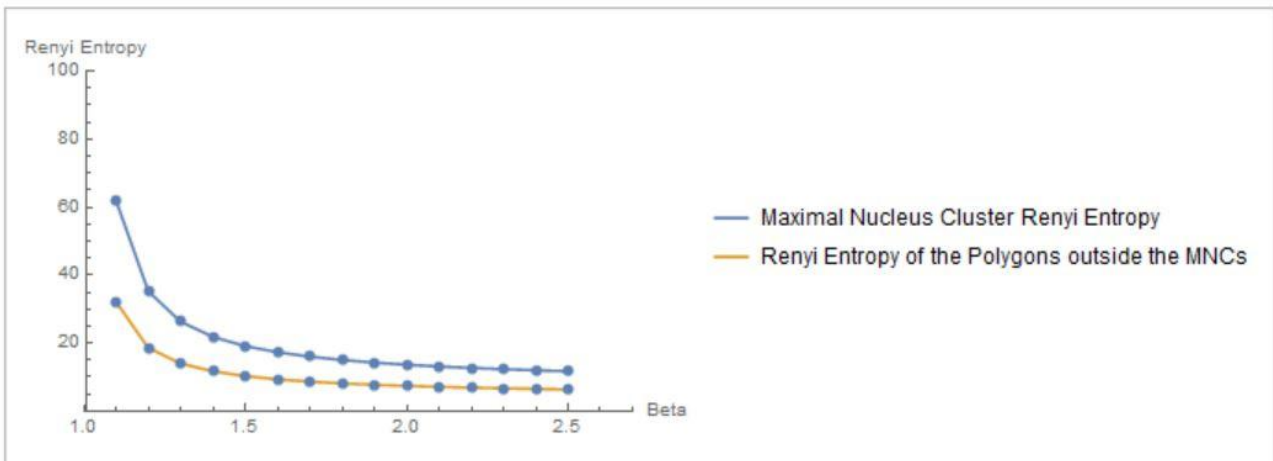


**Figure 3**. Rényi entropy values of maximal nucleus clusters, compared with the surrounding areas of cosmic images. The $x$ axis displays the values of the Beta parameter for $1.1 \leq \beta \leq 2.5$.

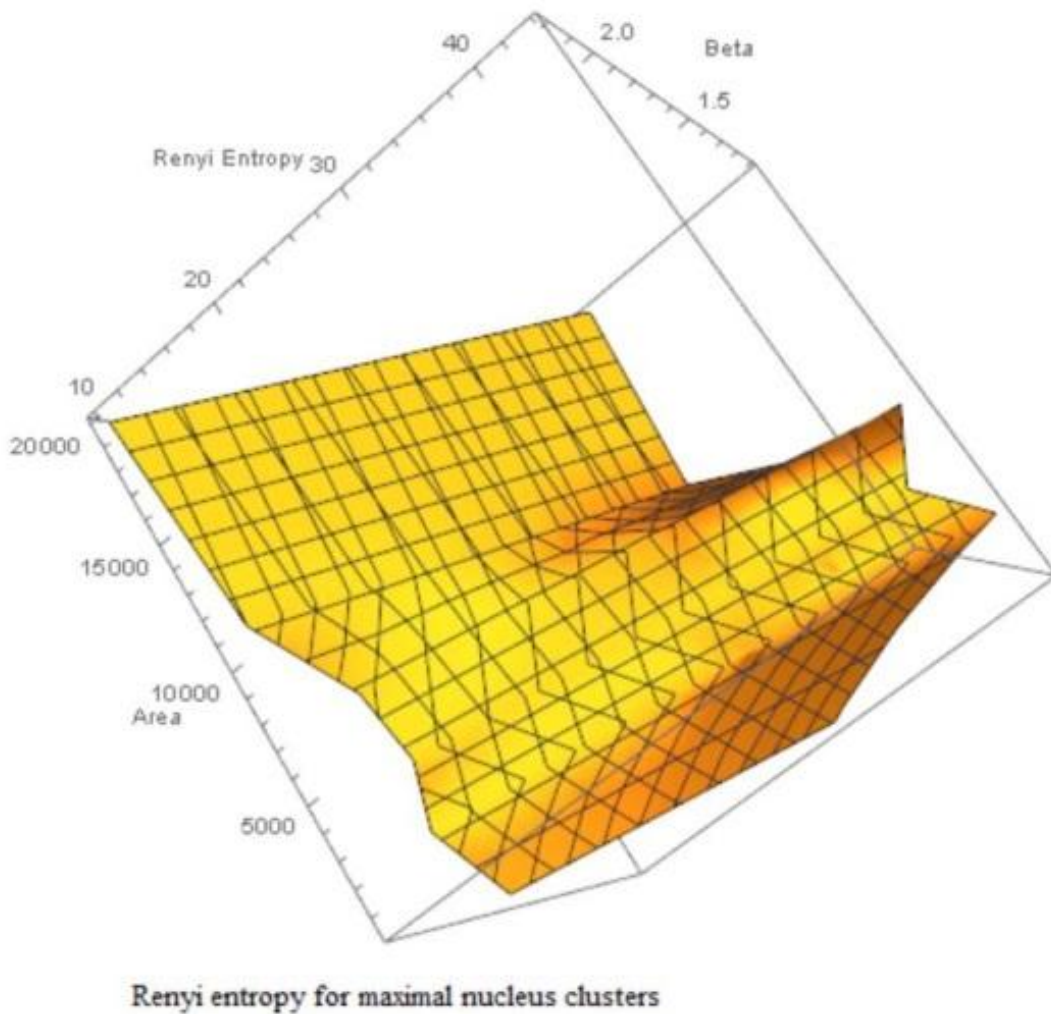**Renyi entropy for maximal nucleus clusters**

**Figure 4**. Rényi entropy values vs. number polygon areas vs. $1.1 \leq \beta \leq 2.5$ of maximal nucleus clusters in cosmic images. MNC Nuclei surrounded by polygons with smaller areas have higher Rényi entropy, which tells us that smaller MNC areas yield more information than MNCs with larger areas.

In sum, Rényi entropy provides a measure of the information in maximal nucleus clusters and the surrounding zones of cosmic images. This means that the information from areas occupied by MNCs vs. non-MNC areas can be measured and compared. This also means that the maximal nucleus clusters are equipped with higher entropy values (and corresponding higher information), which contrasts with measure of information in the surrounding non-MNC zones. Hence, MNCs make it possible to pinpoint the highest source of information in images of the Universe.

**Dark matter comes into play.** MNCs indicate zones where singular generating points lie which are equipped with gradient orientations and gradient magnitudes different from the rest of the cosmic image. This means, in our case, that the homogeneity of the galaxies is broken in some points, where a different gradient orientation angle occurs. A deformation of the spacetime occurs in the zones of MNCs. What is the cause of such local inhomogeneities? We can assess the discrepancies in terms of symmetry breaks, locally disrupting the general symmetry of the cosmic structures' experimentally detected movements. Symmetries, in turn, are dictated by the mutual interactions between visible and dark matter. Symmetry breaks could be due to factors that obstruct the natural settings of stars in galaxies, which results from the subtle interaction of visible and dark masses. Indeed, a variant of the virial theorem (Pollard, 1964) states that:

$$v = \sqrt{GM/r}$$

where v is the velocity of stars, G is the gravitational constant, M is the mass and r is the distance of the star from the center of the galaxy. It means that an increase of dark matter, believed as located out of the galaxies, increases the value of the mass M, in order that stars speed v does not decrease as could be expected when their distance r from the center of the Galaxy increases. Therefore, MNCs might stand for zones where the ratio visible/dark matter is different, compared with others. It leads to the subtle differences in gradient orientation detected by MNCs. In sum, the concentration of dark

matter in MNCs cosmic zones is different from the surrounding ones. The next answer is: once established that in MNCs zones the concentration of dark matter is diverse from the surrounding zones, could we assess whether it is higher or lower? The increase of Rényi entropy in the MNCs zones suggests that information is higher into such zones and lower outside. Because visible matter is detectable, while dark matter is not, it is expected that an increase in information in MNCs is dictated by larger concentrations of visible matter. In sum, MNC zones contain more visible matter than the surrounding zones, and it means less dark matter. In sum, MNCs in a tessellated cosmic image point to cosmic regions that has a diminished presence of dark matter.

## RESULTS

At first, we evaluated the presence of MNC in the coarse graining, large-scale image of the cosmic microwave background (**Figure 2A**). We found that MNSs, rather than being scattered everywhere, are localized in clusters embedding specific zones of the Universe. It is noteworthy that the MNC pattern is not as isotropic as the microwave background. The SDSS 3-dimensional map displays instead a symmetrical pattern of MNCs (**Figure 2B**). Note that the maximal nuclei lie in zones with lesser concentration of galaxies. The MNC tessellation of more recent, lower-scale cosmic bodies (**Figure 3**), revealed that MNCs, rather than being embedded in the very core of the galaxies, generally lie in their outer branches. Note that the MNCs are generally not embedded in the youngest astronomic bodies (see, e.g., **Figure 1**). Clusters of MNCs micro-zones are scattered throughout the pictures (**Figures 4** and **5**). In order to quantitatively assess MNCs' size, we also provided the nuclei areas in square light years (see the legends of **Figures 2 and 3**). Interestingly, the galactic zones containing black holes displayed less MNCs than the surrounding structures (**Figure 5**). In sum, MNCs clusters, equipped with higher Rényi entropy compared with the surrounding zones, are scattered throughout different cosmic areas. It means that some micro-areas of a specific cosmical zones contain more information than the adjacent ones.

## CONCLUSIONS

We showed that computational proximity (i.e., strongly near nucleus mesh clusters) is able to reveal, in 2D fMRI images, hidden patterns of Rényi entropy, enabling us to detect functional information from morphological data. There is a difference in Rényi entropy between MNC and the surrounding zones, these data pointing towards diverse levels of dark matter. Therefore, in different coarse-grained images of the Universe at different times of evolution, MNC is able to detect the presence of zones in which the concentration of dark matter is lower. This result paves the way towards novel approaches to cosmological evaluation, because MNC elucidates the zones of the Universe more likely to contain dark matter. MNC tessellation allows us to confine the zones of the sky in looking for such elusive matter: this could also help reduce the number of dark matter candidates. The holographic principle states that informational content of all the objects that have fallen into a black hole might be entirely contained in surface fluctuations of the event horizon (Susskind, 2004; Pourhasan et al., 2014). It means that the black hole surface needs to have less information than the surrounding cosmological structures. Our data show that this is the case: indeed, in the zones of the black hole, the information is lower. In conclusion, by uncovering evidence of dark matter in different cosmic images, our study shows that a novel and fairly inexpensive image-analysis technique of simple planar images gives insights into the expansion of the Universe. Further, MNC allows the detection of informational entropy which does not necessarily correspond to the zones of the image that we repute more significant. This means that MNC provide a basis for quantifying high-yield information areas in cosmic image features that are normally "hidden" from our attention.
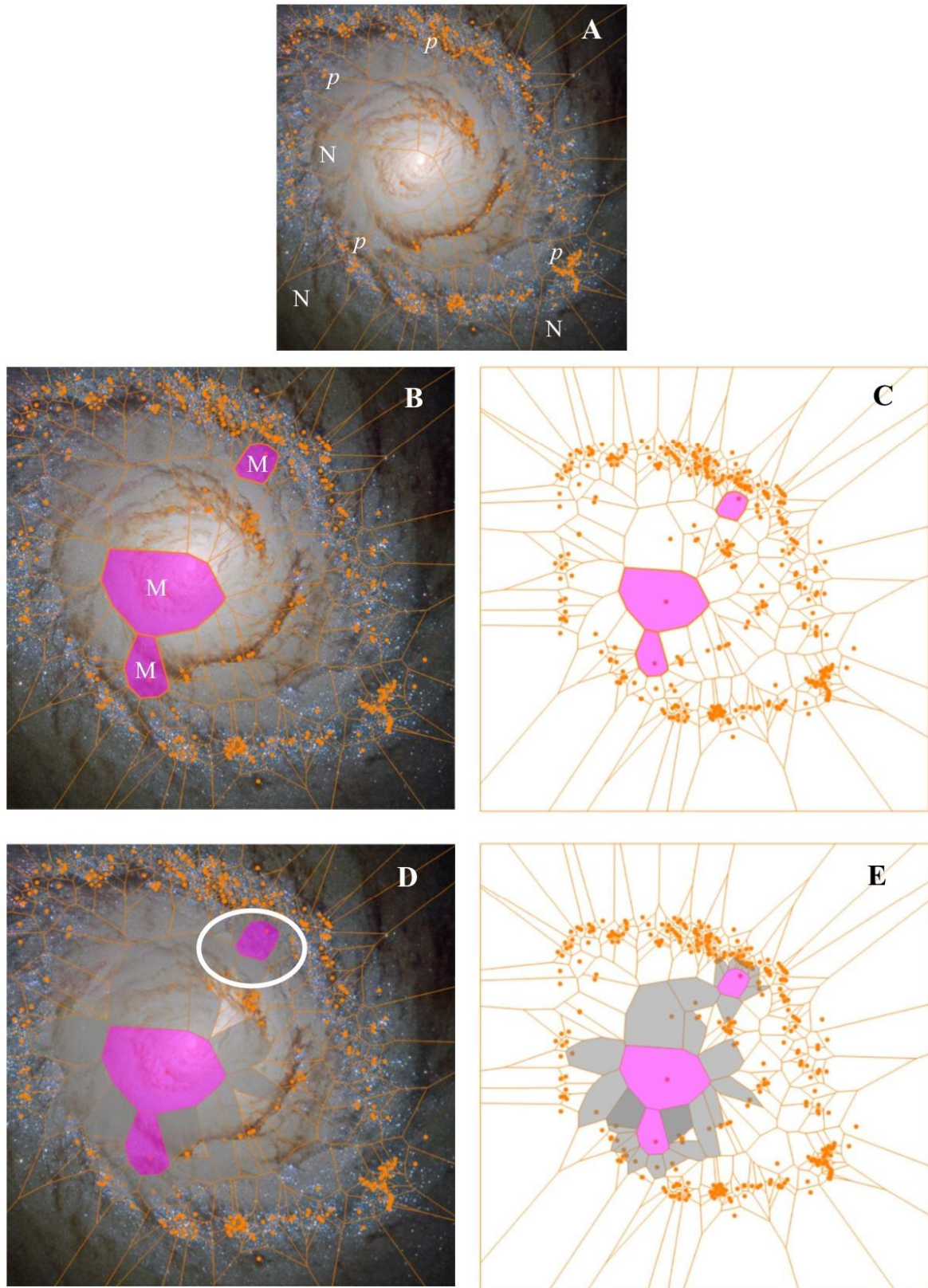
**Figure 1**. Computational proximity methods on a cosmic image (Starburst Galaxy Messier 94). **Figure 1A** depicts a Voronoï tessellation, **Figure 1B** three cluster nuclei and **Figure 1C** their surface tiling (without the original picture), which allows an easier evaluation. **Figure 1D** shows the three maximal nucleus clusters and **Figure 1E** their surface tiling. See main text for further details.
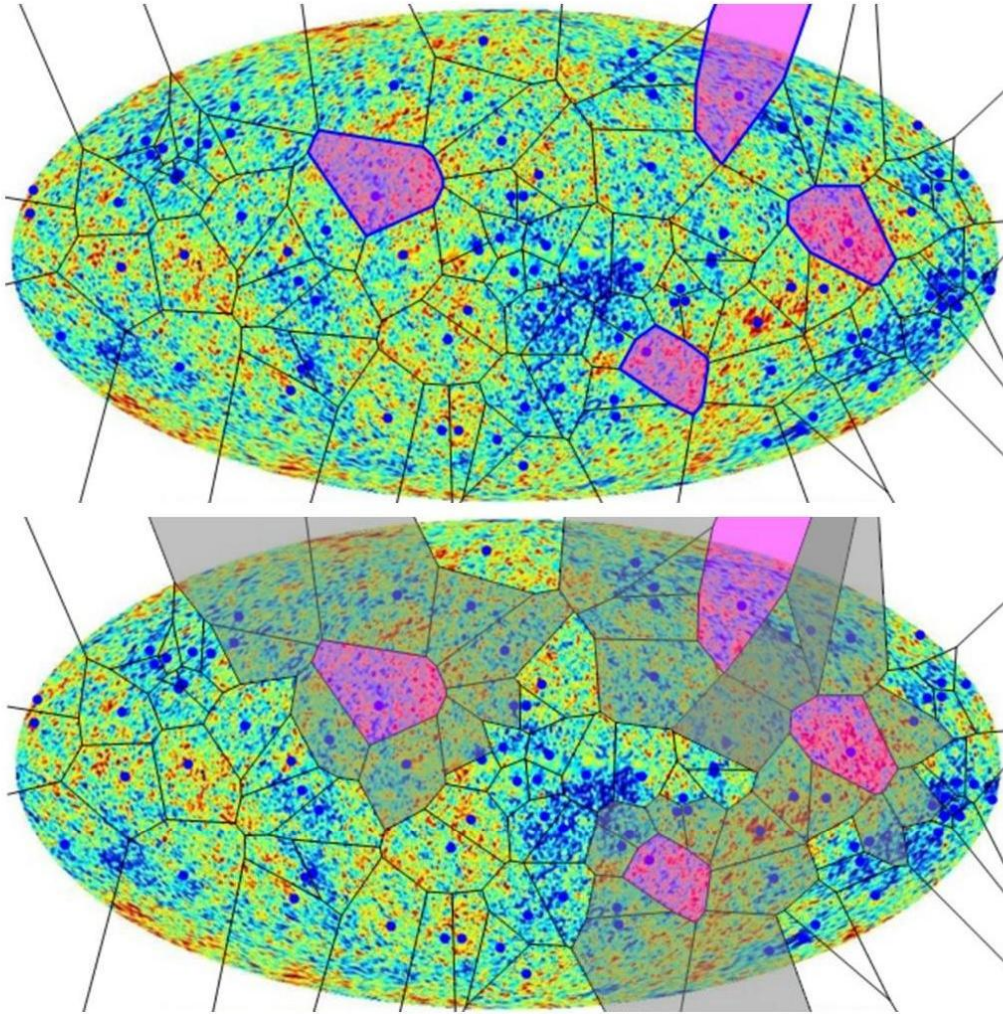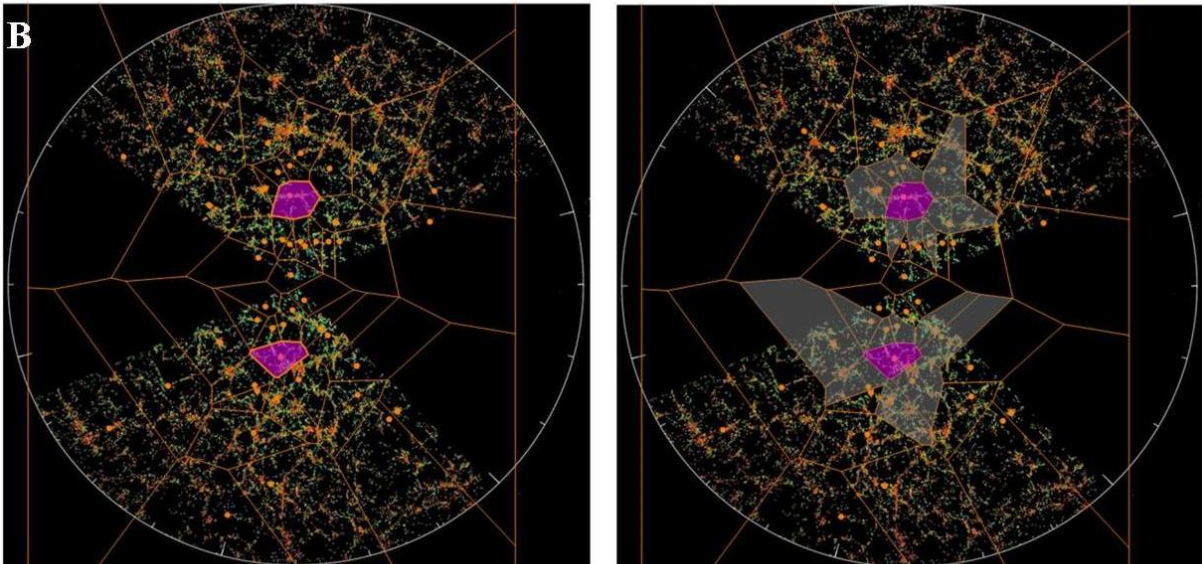
**Figure 2A**: cluster nuclei and MNC of a picture taken from the cosmic microwave background. **Figure 2B**: cluster nuclei and MNC of a picture taken from the SDSS 3-dimensional map of the distribution of galaxies.
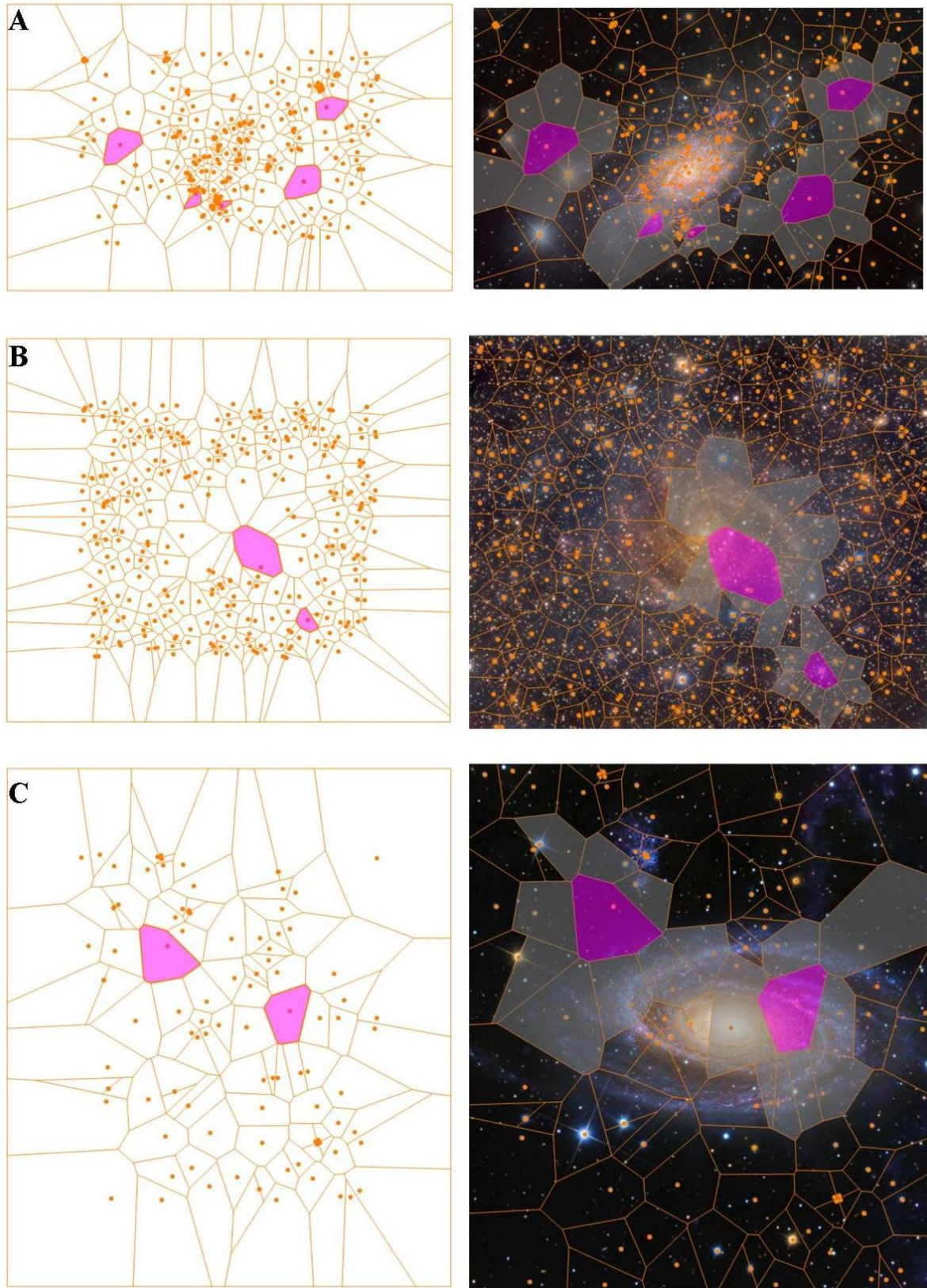
**Figure 3**. Cluster nuclei and MNC of pictures taken from different cosmic structures. **Figure 3A**: NGC 2403. The nuclei areas in square light years (ltyr$^2$) are: N1 area= 14979.1 ltyr$^2$; N2= 14861.9; N3 = 9074.54; N4 = 2774.25; N5= 1179.78. The nuclei are marked with numbers (not shown in Figure) N1-N5 from right to left. **Figure 3B**: the Hidden Galaxy IC 342. Nuclei areas: N1 = 29375.9, N2 = 5624.46. **Figure 3C:** IRG-NGC303 Galaxy. Nuclei areas: N1 = 21654.8, N2 = 17403.7.
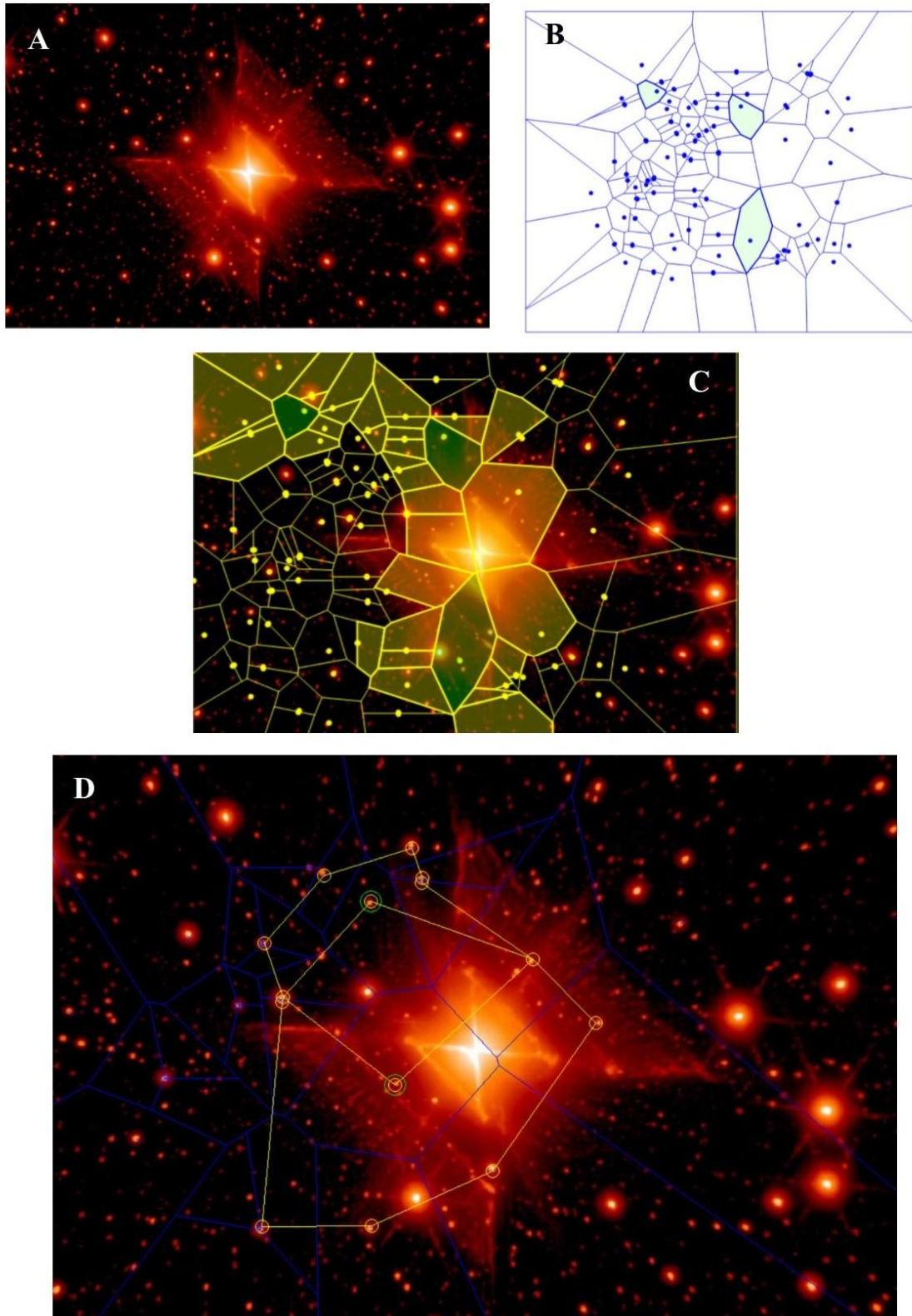
**Figure 4.** Tessellation of the Red Square Nebula MWC9 22. **Figure 4A** illustrates the original image, **Figure 4B** its three cluster nuclei and **Figure 4C** the corresponding three MNCs. **Figure 4D** shows two Voronoï nuclei. The concentric circles represent nuclei generating points, while the non-concentric circles (endpoints of the straight edges in this mesh) are the generating points of the adjacent Voronoï regions. This means that this pair of MNCs overlaps.
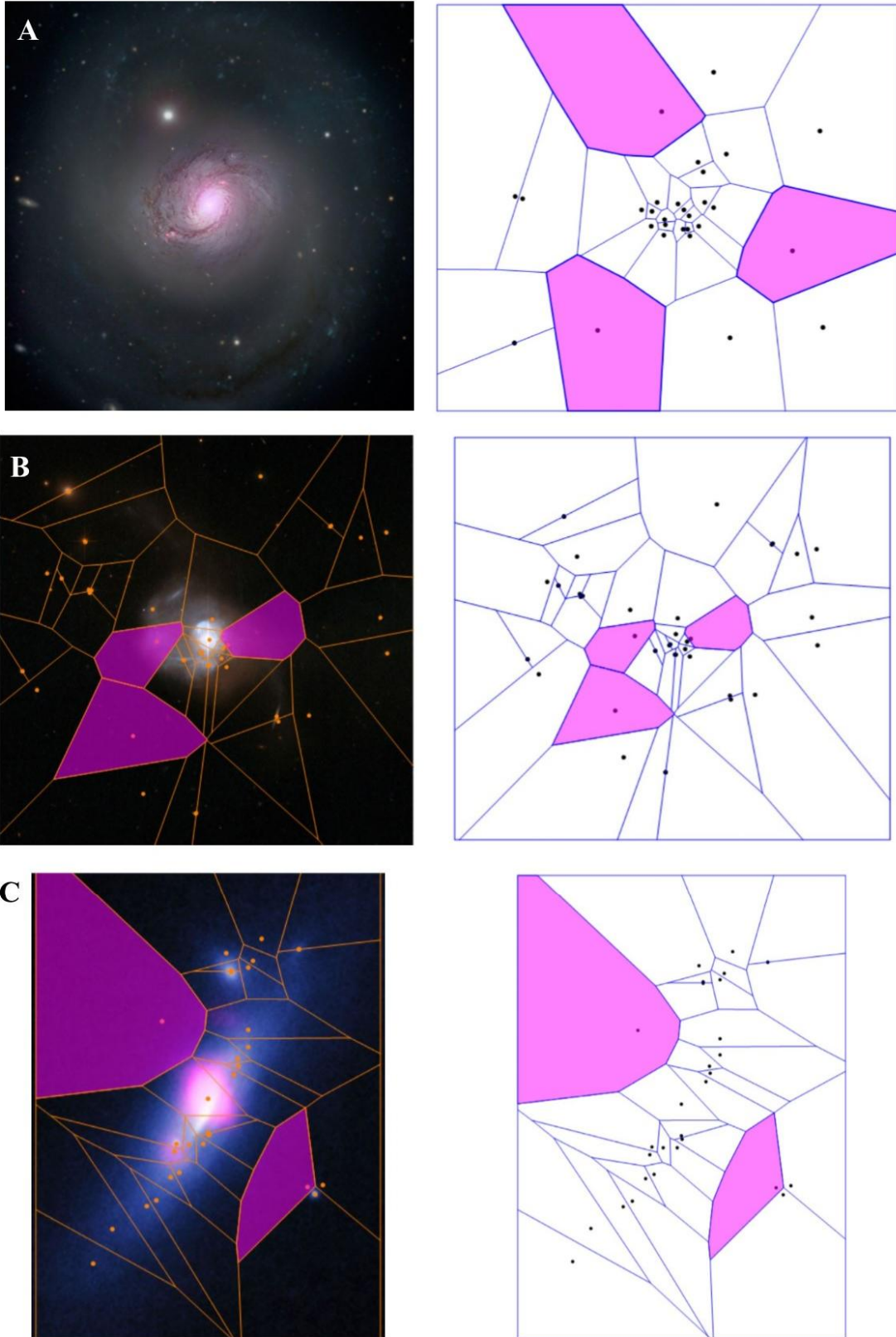
**Figure 5**. Tessellation of three different galactic structures containing black holes: NGC 1068 (**Figure 5A**), Markarian231 (**Figure 5B**) and SDSSK1126-2944 (**Figure 5C**). Note that the MNCs always occur outside the black holes.

**REFERENCES**

1) Aad G, Abajyan T, Abbott B, Abdallah J, Abdel Khalek S, et al. 2013. Search for dark matter candidates and large extra dimensions in events with a photon and missing transverse momentum in pp collision data at 7 TeV with the ATLAS detector. Phys Rev Lett. 110(1):011802. Epub 2013 Jan 3.

2) Bromiley PA, Thacker NA, Bouhova-Thacker E. 2010. Shannon entropy, Renyi entropy, and information. Tina 2004-004, Statistic and Inf Series, Imaging Sci. and Biomed. Eng., Univ. of Manchester, UK

3) Edelsbrunner H. 2006. Geometry and Topology for Mesh Generation (Cambridge University Press, Cambridge, U.K.)

4) Edelsbrunner H. 2014. A Short Course in Computational Geometry and Topology (Springer Briefs in Applied Sciences and Technology, Springer, Cham)

5) Fixsen DJ. 2009. The Temperature of the Cosmic Microwave Background. The Astrophysical Journal 707 (2): 916–920. doi:10.1088/0004-637X/707/2/916.

6) Frank NP, Hart SM. 2010. A dynamical system using the Voronoï tessellation. The Amer Math Monthly 117(2):92–112.

7) Gawiser E, Silk J. 2000. The cosmic microwave background radiation. Physics Reports. 333–334: 245–267. doi:10.1016/S0370-1573(00)00025-9.

8) Khachatryan V, Sirunyan AM, Tumasyan A, Adam W, Bergauer T, et al. 2015. Search for dark matter, extra dimensions, and unparticles in monojet events in proton-proton collisions at … Eur Phys J C Part Fields. 75(5):235. Epub 2015 May 29.

9) Penrose R. 2011. Cycles of Time. An Extraordinary New View of the Universe. Alfred A. Knopf, NY, 2011.

10) Penzias AA, Wilson RW. 1965. A Measurement of Excess Antenna Temperature at 4080 Mc/s. The Astrophysical Journal 142 (1): 419–421. doi:10.1086/148307.

11) Peters JF, Guadagni C. 2015. Strong proximities on smooth manifolds and Voronoi diagrams, Advances in Math. 4, no. 2, 97-107.

12) Peters JF. 2016. Computational Proximity. Excursions in the Topology of Digital Images. (Springer, Intelligent Systems Reference Library 102, Berlin, ISBN 978-3-319-321662), *in press*.

13) Peters JF, İnan E. 2016. Strongly near Voronoï nucleus clusters. arXiv 1602(03734): 1-7.

14) Peters JF, Tozzi A. Ramanna S. 2016. Brain Tissue Tessellation Shows Absence of Canonical Microcircuits. Neuroscience Letters 626: 99–105. doi:10.1016/j.neulet.2016.03.052.

15) Pollard H. 1964. A sharp form of the virial theorem. Bull. Amer. Math. Soc. LXX (5): 703–705.

16) Pourhasan R, Afshordi N, Mann RB. 2014. Out of the white hole: a holographic origin for the Big Bang. Journal of Cosmology and Astroparticle Physics. JCAP04(2014)005 (http://iopscience.iop.org/1475-7516/2014/04/005)

**17)** Rényi A. 1961. On measures of entropy and information. Proc. Fourth Berkeley Symp. Math. Stat. and Probability, vol. I, Berkeley, CA, University of California Press, 547-457, MR0132570**.**

18) Rényi A. 1966. On the amount of information in a random variable concerning an event. J. Math. Sci. 1, 30-33, MR0210263.

19) Rényi A. 1982. Tagebuch über die Informationstheorie. VEB Deutcher der Wissenschaften, Berlin, 173 pp., MR0707097.

20) Saye RI, Sethian JA. 2011. The Voronoi implicit interface method for computing multiphase physics. Proc. Nat. Acad. of Sci. 108(49): 19498-19503, doi/10.1073/pnas.111155708.

21) Susskind L. 2004. An Introduction to Black Holes, Information and the String Theory Revolution: The Holographic Universe. (World Sci. Pub., Singapore, ISBN-13 978-9812561312).

22) van de Weygaert R. 2007. Voronoi Tessellations and the Cosmic Web: Spatial Patterns and Clustering across the Universe. arXiv:0707.2877v1.